ELSEVIER

Thermochimica Acta 342 (1999) 7–18

thermochimica acta

www.elsevier.com/locate/tca

Dynamic heat capacity measurements in advanced AC calorimetry

A.A. Minakov[a,*], Yu.V. Bugoslavsky[a], C. Schick[b]

[a]*General Physics Institute, R.A.S., Vavilov st. 38, 117942 Moscow, Russia*
[b]*Department of Physics, University of Rostock, Universitatsplatz 3, 18051 Rostock, Germany*

Received 25 1999; received in revised form 13 1999; accepted 13 1999

Abstract

The new capabilities of AC calorimetry, when working at frequencies above the classical limit, were shown. The idea of the method was to use the information about the phases and the amplitudes of the temperature oscillations on both sides of a plate-like sample for *simultaneous* determination of the sample's complex heat capacity $\mathbf{C}_s(\omega)$ and thermal conductivity $\boldsymbol{\kappa}_s(\omega)$, when the oscillating heat flow was supplied to one face of the sample. The mathematical algorithm for simultaneous determination of real and imaginary parts of the sample's heat capacity and thermal conductivity was developed. The advanced AC technique was applied for polymers. As a first step, the approximation of the frequency independent thermal conductivity was used to determine the complex heat capacity $\mathbf{C}_s(\omega)$ of polymers in the melting region. It was found that the processes of reversing (more definitely heat-reversing) melting and completely irreversing melting can be distinguished by the complex heat capacity measurements. Thus, the different physical processes at melting can be distinguished by the complex heat capacity measurements. © 1999 Elsevier Science B.V. All rights reserved.

Keywords: AC calorimetry; Complex heat capacity; Thermal conductivity; Temperature-modulated calorimetry; Melting dynamics; Polymers

1. Introduction

The general scheme of AC calorimetry measurements is to supply an oscillating heat flow $P_0 \cdot \cos(\omega t)$ to one side of the sample, and to measure the temperature oscillations $T_0 \cdot \sin(\omega t + \varphi)$ on the other side [1–4]. Recently, the new capabilities of AC calorimetry, when working at frequencies above the classical limit, were demonstrated [5,6]. At high frequencies, the temperature oscillations in the sample are not quasi-static, i.e. $\varphi \neq 0$. The idea of the method [5] was to use the information about both the phase and the amplitude of the temperature wave transmitted through a plate-like sample for simultaneous determination of the sample's heat capacity C_s and the thermal conductivity κ_s. The mathematical algorithm to do so was presented in the paper [5]. The advanced AC calorimetry was applied to studies of polymers in [5,6].

The aim of this work is to further advance AC technique, for time-dependent or frequency-dependent heat capacity measurements. Heat capacity becomes complex and frequency dependent, when a slow relaxation process occurs in the system. The presence of the imaginary part of heat capacity inevitably leads to the entropy production during the cycling of the sample's temperature [7–10]. On the other hand, if the irreversing melting occurs in the system, the non-zero imaginary part of heat capacity

*Corresponding author. Fax: +7-95-135-82-81
E-mail address: minakov@ran.gpi.ru (A.A. Minakov)

0040-6031/99/$ – see front matter © 1999 Elsevier Science B.V. All rights reserved.
PII: S0040-6031(99)00298-1

must be measured, as it was shown in [11,5]. The complex heat capacity $\mathbf{C}_s(\omega)$ of a sample can be measured by AC calorimeter in the appropriate frequency range. Using the information about the amplitudes T_{01} and T_{02} as well as the phases φ_1 and φ_2 on both sides of the sample, it is possible to obtain *simultaneously* the complex heat capacity $\mathbf{C}_s(\omega)$ and the complex thermal conductivity $\boldsymbol{\kappa}_s(\omega)$, i.e. four parameters: Re($\mathbf{C}_s$), Im($\mathbf{C}_s$), Re($\boldsymbol{\kappa}_s$) and Im($\boldsymbol{\kappa}_s$). The mathematical algorithm to do so is presented in the first part of this paper.

Next, we focus on the complex heat capacity, $\mathbf{C}_s = C_s \exp(-i\phi)$, and consider the approximation of the frequency independent sample's thermal conductivity $\boldsymbol{\kappa}_s$. To determine the parameters Re($\mathbf{C}_s$) and Im($\mathbf{C}_s$) simultaneously, it was sufficient to measure temperature modulation only on one side of the sample. In our experiments the temperature modulation was measured on that side of the sample, which was opposite to the heated sample's surface. In this case, it was possible to determine $\boldsymbol{\kappa}_s(T)$ in the temperature region far from phase transitions, where $\mathrm{Im}(\mathbf{C}_s) = 0$. In general, the phase shift φ was a sum of two contributions. The first contribution was equal to $\phi = \arg\{1/\mathbf{C}_s(\omega)\}$. This was a positive contribution to the phase shift φ. Note, that by definition $\mathbf{C}(\omega) = C' - iC''$, where $C'' > 0$. The second contribution was equal to the phase lag $\varphi_{\boldsymbol{\kappa}}$, depending on the system thermal conductivity. This contribution was negative and tended to $-\infty$, when the thickness of the sample and/or modulation frequency were increased. Consequently, it was possible to distinguish these two contributions, which were opposite in sign.

Of course, it was impossible to separate three parameters Re $\mathbf{C}_s$, Im $\mathbf{C}_s$, $\boldsymbol{\kappa}_s$, when only two, T_0 and φ, were measured. However, it was possible to determine the large maxima of Re $\mathbf{C}_s(T)$ and Im $\mathbf{C}_s(T)$ near phase transitions. In the first approximation, we extrapolated the smooth temperature dependence of thermal conductivity from the temperature regions, where Im $\mathbf{C}_s = 0$. Thus, it was assumed that the dynamic contribution to the thermal conductivity was relatively small. The sample's thermal conductivity in the temperature range around the phase transition was determined by the algorithm described in [5]. Then, the thermal conductivity was extrapolated on the whole temperature range. These results were in good agreement with the steady-state measurements of $\boldsymbol{\kappa}_s(T)$. The extrapolated dependence $\boldsymbol{\kappa}_s(T)$ was used for the calculations of Re $\mathbf{C}_s(T)$ and Im $\mathbf{C}_s(T)$ from the measured temperature dependences of the modulation amplitude and the phase shift. The algorithm for these calculations was developed and applied to polymers in the melting region. The excess heat capacity $\mathbf{C}_{ex}$ related to the latent heat can be measured in the melting region. The real and imaginary parts of the excess heat capacity $\mathbf{C}_{ex}$ in the melting region were measured. The two types of the melting process were observed. The first type, when the excess heat capacity is mainly real valued, $\mathrm{Re}(\mathbf{C}_{ex}) >> \mathrm{Im}(\mathbf{C}_{ex})$, can be named as ''reversing melting'' [12] or, may be more definitely, as ''heat-reversing melting''. The second, when $\mathrm{Re}(\mathbf{C}_{ex}) = 0$, corresponds to the completely irreversing melting. The term ''heat-reversing melting'' can be used to emphasize that the heat absorbed at heating is released at cooling in each temperature-modulation cycle. Of course, it does not mean reversibility in microscopic scale.

2. The method: general description

The construction of the calorimeter was described in [5,13]. The calorimeter cell — the system for creation and registration of temperature modulation in a disk-shaped sample — consists of a heater, a sensor, and a holder. The sample is placed between the heater and the sensor substrates. The heater and the sensor are formed on the surfaces of polished sapphire disks of 3 mm diameter and of thickness 0.1 mm. The heater is a chromium film, sputtered on the first sapphire substrate. Copper contact pads are sputtered on the film, and copper wires of 50 μm diameter are welded to the pads. The power of the resistive heater equals $P_0 \cdot (1 + \cos \omega t)$, where $\omega/2$ is the angular frequency of the electric current and P_0 the average power of the heater. To form the sensor, a copper field is sputtered on the second sapphire substrate. The thermocouple (Cu–Cu:Fe) wires of 50 μm diameter are welded to the copper field. The sensor is glued on a silk net, which serves as a holder. Thus, the system consists of four layers, including the sample.

This layered system is heated by a uniform heat flow of oscillating rate $P = P_0 \cdot \cos(\omega t)$. The flow is supplied to the outer face of the first layer at $z = 0$ and propagates through the system along the z-axis. The

cross area S of the system is independent on z. Provided the heat leakage through the perimeter of the system is negligible, the plane temperature waves $T = \mathrm{Re}[T_0 \cdot \exp(\mathrm{i}\omega t \pm \mathbf{k}z)]$ propagate across the system, where $\mathbf{k} = \exp(\mathrm{i}\pi/4) \cdot (\omega \mathbf{c}/\boldsymbol{\kappa})^{1/2}$, $\mathbf{c}$ is the specific heat capacity and $\boldsymbol{\kappa}$ the thermal conductivity of the material. In general, $\mathbf{c}$ and $\boldsymbol{\kappa}$ are the complex values: $\mathbf{c} = c \exp(-\mathrm{i}\phi)$, $\boldsymbol{\kappa} = \kappa \cdot \exp(-\mathrm{i}\vartheta)$. Note that the complex values are expressed in bold font and the modulus in Italic. The negative signs of the phases of $\mathbf{c}$ and $\boldsymbol{\kappa}$ mean the delay in the system response. Strictly speaking, the square root of a complex value is double valued. Thus, one should consider the following two possibilities: $(\mathbf{c}/\boldsymbol{\kappa})^{1/2} = \exp(-\mathrm{i}\phi/2 + \mathrm{i}\vartheta/2) \cdot (c/\kappa)^{1/2}$ and $(\mathbf{c}/\boldsymbol{\kappa})^{1/2} = \exp(-\mathrm{i}\phi/2 + \mathrm{i}\vartheta/2 + \mathrm{i}\pi) \cdot (c/\kappa)^{1/2}$. The second branch of the complex function $(\mathbf{c}/\boldsymbol{\kappa})^{1/2}$ has no physical meaning, because the physical values, $\mathbf{c}$ and $\boldsymbol{\kappa}$ as well as ϕ and ϑ, are varied continuously with temperature and frequency. Indeed, the square root $(\mathbf{c}/\boldsymbol{\kappa})^{1/2}$ must be real valued far from phase transitions, at $\phi = 0$ and $\vartheta = 0$, when the specific heat capacity and the thermal conductivity are real valued. Therefore, only the first branch of $(\mathbf{c}/\boldsymbol{\kappa})^{1/2}$ should be considered.

Consider the approximation of the long temperature waves, $k^{-1} \gg \lambda_{\mathrm{ph}}$, where λ_{ph} is a phonon free path. This approximation is valid for polymers below 10^5 Hz at room temperature. In this frequency domain the heat transfer equation without heat sources is as follows: $\mathbf{c} \cdot \partial T/\partial t = \partial/\partial z(\boldsymbol{\kappa} \cdot \partial T/\partial z)$. In the linear approximation, when $(\kappa)^{-1} \cdot (\partial \kappa/\partial T) \cdot T_0 << 1$, this equation can be approximated by the equation $\mathbf{c} \cdot \partial T/\partial t = \boldsymbol{\kappa} \cdot \partial^2 T/\partial z^2$. This approximation can be applied at sufficiently small amplitudes $T_0 << \Delta T_{\mathrm{tr}}$, where ΔT_{tr} is the width of the phase transition. The stationary oscillating solution of this heat transfer equation is $\mathrm{Re}\{\exp(\mathrm{i}\omega t) \cdot [\mathbf{a} \cdot \sinh(\mathbf{kz}) + \mathbf{b} \cdot \cosh(\mathbf{kz})]\}$. Therefore, the temperature wave $\mathbf{T}_i(z) = \exp(\mathrm{i}\omega t) \cdot \{\mathbf{a}_i \cdot \sinh[\mathbf{k}_i(z - \xi_i)] + \mathbf{b}_i \cdot \cosh[\mathbf{k}_i(z - \xi_i)]\}$ is excited in the ith layer, where ξ_i is the coordinate of ith boundary. The complex coefficients $\mathbf{a}_i$ and $\mathbf{b}_i$ are determined by boundary conditions for temperature and heat flow amplitudes on the faces of the ith layer. The complex amplitude $\mathbf{T}_{0i}$ of the temperature modulation on the ith surface equals $\mathbf{b}_i$.

In general, the following effective heat capacity is measured in classical AC calorimetry:

$$\mathbf{C}_{\mathrm{eff}} = P_0/(\mathrm{i}\omega \mathbf{T}_{\mathrm{A}}), \tag{1}$$

which is proportional to the heat-flow amplitude P_0 and inversely proportional to the measured complex amplitude $\mathbf{T}_{\mathrm{A}}$. Of course, at sufficiently low frequencies and sufficiently low heat-link between the system and the thermostat the effective heat capacity $\mathbf{C}_{\mathrm{eff}}$ equals the sum of the sample's heat capacity $\mathbf{C}_{\mathrm{s}}$ and the heat capacity of the empty cell. The phase shift between the temperature modulations in the heater and in the sensor equals zero at these conditions. In fact, the phase shift between the heat-flow and $\mathbf{T}_{\mathrm{A}}$ equals φ - $\pi/2$. As the trivial phase lag $\pi/2$ is not of interest, we consider the phase shift $\varphi = \arg(1/\mathbf{C}_{\mathrm{eff}})$. This phase shift tends to zero at low frequencies and far from phase transitions. In general, the relation between the measured $\mathbf{C}_{\mathrm{eff}}$ and $\mathbf{C}_{\mathrm{s}}$ is complicated.

The general solution of the heat transfer equation for the system of n layers was obtained in [5], for the case of the heat leakage into the wires of the thermocouple and through the perimeter of the system being negligible. Denote the effective heat capacity $\mathbf{C}_{0i} = P_0/(\mathrm{i}\omega \mathbf{T}_{0i})$ related to the amplitude $\mathbf{T}_{0i}$. The effective heat capacities $\mathbf{C}_{01}$ and $\mathbf{C}_{0n}$, measured on the first and on the nth surfaces of the system, can be expressed as follows:

$$\begin{aligned} \mathbf{C}_{01} &= [\mathbf{B}_{\mathrm{odd}} + G/\mathrm{i}\omega]/[1 + \mathbf{B}_{\mathrm{even}}], \mathbf{C}_{0n} \\ &= [\mathbf{B}_{\mathrm{odd}} + G/\mathrm{i}\omega] \cdot \cosh(\boldsymbol{\alpha}_1) \ldots \cosh(\boldsymbol{\alpha}_{n-1}), \end{aligned} \tag{2}$$

where G is a constant, characterizing the heat-link between the system and the thermostat and $\boldsymbol{\alpha}_i = d_i \cdot \mathbf{k}_i$ the parameter characterizing the thermal length of the ith layer of thickness d_i. The terms of odd power of $\boldsymbol{\alpha}_i$ are presented by the sum $\mathbf{B}_{\mathrm{odd}} = \mathbf{B}_1 + \mathbf{B}_3 + \cdots + \mathbf{B}_{2m+1}$, where $2m + 1 \leq n$, and the terms of even power by the sum $\mathbf{B}_{\mathrm{even}} = \mathbf{B}_2 + \mathbf{B}_4 + \cdots + \mathbf{B}_{2m}$, with $2m \leq n$. Denote $\boldsymbol{\beta}_{ba} = \boldsymbol{\kappa}_b \mathbf{k}_b / \boldsymbol{\kappa}_a \mathbf{k}_a$, i.e. $\boldsymbol{\beta}_{ba} = (\mathbf{C}_b \cdot \boldsymbol{\alpha}_a)/(\mathbf{C}_a \cdot \boldsymbol{\alpha}_b)$, where $\mathbf{C}_l$ is the heat capacity of the lth layer. Then, $\mathbf{B}_i$ can be written as follows:

$$\begin{aligned} \mathbf{B}_1 &= \sum (\mathbf{C}_a/\boldsymbol{\alpha}_a) \cdot \tanh(\boldsymbol{\alpha}_a), \\ \mathbf{B}_2 &= \sum \boldsymbol{\beta}_{ba} \cdot \tanh(\boldsymbol{\alpha}_a) \cdot \tanh(\boldsymbol{\alpha}_b), \\ \mathbf{B}_3 &= \sum (\mathbf{C}_a/\boldsymbol{\alpha}_a) \cdot \boldsymbol{\beta}_{cb} \cdot \tanh(\boldsymbol{\alpha}_a) \cdot \tanh(\boldsymbol{\alpha}_b) \cdot \tanh(\boldsymbol{\alpha}_c), \\ \mathbf{B}_4 &= \sum \boldsymbol{\beta}_{ba} \cdot \boldsymbol{\beta}_{dc} \cdot \tanh(\boldsymbol{\alpha}_a) \cdot \tanh(\boldsymbol{\alpha}_b) \cdot \tanh(\boldsymbol{\alpha}_c) \\ &\quad \cdot \tanh(\boldsymbol{\alpha}_d), \\ \mathbf{B}_5 &= \sum (\mathbf{C}_a/\boldsymbol{\alpha}_a) \cdot \boldsymbol{\beta}_{cb} \cdot \boldsymbol{\beta}_{ed} \cdot \tanh(\boldsymbol{\alpha}_a) \cdot \tanh(\boldsymbol{\alpha}_b) \\ &\quad \cdot \tanh(\boldsymbol{\alpha}_c) \cdot \tanh(\boldsymbol{\alpha}_d) \cdot \tanh(\boldsymbol{\alpha}_e), \end{aligned} \tag{3}$$

and so on for all indexes, such that $a < b < c < d < e \ldots$ The sum $\mathbf{B}_q$ is taken over all combinations of q elements from n, i.e. over C_n^q elements.

The terms, which are proportional to the high power of α_i, are negligibly small at low frequencies. Indeed, $\tanh(\boldsymbol{\alpha}_i) \approx \boldsymbol{\alpha}_i$ at small α_i, and α_i decrease with frequency as $\alpha_i \sim \sqrt{\omega}$. Of course, in the low-frequency limit, the zero-order term, $\mathbf{B}_1$, is equal to the sum of the heat capacities of all layers, $\mathbf{B}_1 = \Sigma \mathbf{C}_l$.

3. The method: heater–sample–sensor–holder system

Next we apply the method to study polymer materials. The ideal thermal contact of the sample with the calorimeter cell is assumed. This approximation is sufficient for polymers — the materials with relatively low thermal conductivity, $\kappa_s < 1$ W/m K, as it was shown in [14]. Usually, after the first melting–crystallization cycle, polymers provide a good and stable thermal contact due to good adhesion with substrate. On the other hand, the thermal contact should be ''wet'' in the case when the sample cannot be melted. Thus, when dealing with solids, a good ''wet'' contact can be made by means of a thin layer of lubricant between the sample and substrate. The vacuum grease, apiezon, can be used for a good, reproducible and stable thermal contact, as it was shown in [14]. To focus on complex heat capacity of polymers, we consider the frequency domain 0.1–10 Hz appropriate for these measurements with the samples of thickness in the range 0.1–0.5 mm.

Consider the heater–sample–sensor–holder system consisting of four layers. Note that the heater and the sensor are formed on the equal sapphire substrates. That is why, we denote by C_0 and d_0 the total heat capacity and the total thickness of two substrates, by c_0 and κ_0 the specific heat capacity and the thermal conductivity of sapphire. Denote the corresponding parameters of the holder and sample with subscripts h and s. In the case of four layers, $n = 4$, the sum $\mathbf{B}_{odd}$ in Eqs. (2) and (3) equals $\mathbf{B}_3$, where $\mathbf{B}_3$ is the sum of four elements. The sum $\mathbf{B}_{even}$ equals $\mathbf{B}_2 + \mathbf{B}_4$, where $\mathbf{B}_2$ is the sum of six elements, and $\mathbf{B}_4$ of one element.

Consider Eqs. (2) and (3) at modulation frequency $f = \omega/2\pi$ below 10 Hz, when $\boldsymbol{\alpha}_0 \ll 1$ and $\tanh(\boldsymbol{\alpha}_0) \approx \boldsymbol{\alpha}_0$. In this case, the cross terms from $\mathbf{B}_2$ and $\mathbf{B}_3$, which are proportional to $\boldsymbol{\beta}_{i0}$, as well as the term from $\mathbf{B}_4$ can be neglected within 3% accuracy. On the other hand, the cross terms from $\mathbf{B}_2$ and $\mathbf{B}_3$, which are proportional to $\boldsymbol{\beta}_{is}$, are essential and should be taken into account. Then, the effective heat capacities $\mathbf{C}_{01}$ and $\mathbf{C}_{04}$, measured on the first and fourth surfaces of the heater–sample–sensor–holder system, can be expressed as follows:

$$\mathbf{C}_{01} = [\mathbf{A} + G/\mathrm{i}\omega + \mathbf{S}_0 + \mathbf{S}_h]/\{1 + [\boldsymbol{\beta}_{0s} \cdot \tanh(\boldsymbol{\alpha}_0/2) + \boldsymbol{\beta}_{hs} \cdot \tanh(\boldsymbol{\alpha}_h)] \cdot \tanh(\boldsymbol{\alpha}_s)\}, \quad (4)$$

$$\mathbf{C}_{04} = [\mathbf{A} + G/\mathrm{i}\omega + \boldsymbol{S}_0 + \boldsymbol{S}_h] \cdot \cosh(\boldsymbol{\alpha}_0) \cdot \cosh(\boldsymbol{\alpha}_s), \quad (5)$$

where $\mathbf{A} = C_0 \cdot \tanh(\boldsymbol{\alpha}_0)/\boldsymbol{\alpha}_0 + C_h \cdot \tanh(\boldsymbol{\alpha}_h)/\boldsymbol{\alpha}_h + \mathbf{C}_s \cdot \tanh(\boldsymbol{\alpha}_s)/\boldsymbol{\alpha}_s$,

$$\mathbf{S}_0 = [\mathbf{C}_s \cdot \tanh(\boldsymbol{\alpha}_s)/\boldsymbol{\alpha}_s] \cdot [(\boldsymbol{\beta}_{0s})^2 - 1] \cdot [\sinh(\boldsymbol{\alpha}_0/2)]^2/\cosh(\boldsymbol{\alpha}_0),$$

$$\mathbf{S}_h = [C_h \cdot \tanh(\boldsymbol{\alpha}_h)/\boldsymbol{\alpha}_h] \cdot (\boldsymbol{\beta}_{0s}/2 + \boldsymbol{\beta}_{s0}/2) \cdot \tanh(\boldsymbol{\alpha}_0) \cdot \tanh(\boldsymbol{\alpha}_s).$$

Of course, the obvious relation $\mathbf{C}_{01} = \mathbf{C}_{04} = (C_0 + C_h + \mathbf{C}_s + G/\mathrm{i}\omega)$ follows from Eqs. (4) and (5) at sufficiently low frequencies. In general, the two complex parameters $\mathbf{C}_s$ and $\boldsymbol{\alpha}_s$ can be determined from the measured $\mathbf{C}_{01}$ and $\mathbf{C}_{04}$, provided other parameters in Eqs. (4) and (5) are known. Finally, the parameter $\boldsymbol{\kappa}_s$ can be determined from the following relation: $\boldsymbol{\kappa}_s = \omega \cdot \mathbf{C}_s \cdot d_s/S \cdot \boldsymbol{\alpha}_s^2$

4. Calibration of the calorimeter

Consider the effective heat capacity $\mathbf{C}_{emp}$ of the empty cell, which is measured on the third surface with respect to the heater. The expression for $\mathbf{C}_{emp}$ follows from Eq. (5) at $\mathbf{C}_s = 0$, $\boldsymbol{\alpha}_s = 0$:

$$\mathbf{C}_{emp} = [\mathbf{C}_0 \cdot \tanh(\boldsymbol{\alpha}_0)/\boldsymbol{\alpha}_0 + \mathbf{C}_h \cdot \tanh(\boldsymbol{\alpha}_h)/\boldsymbol{\alpha}_h + G/\mathrm{i}\omega] \cdot \cosh(\boldsymbol{\alpha}_0). \quad (6)$$

In the above expression, only the parameter G depends on ambient gas pressure. But this dependence is very weak in the pressure range 1–100 Pa. In all measurements the nitrogen gas pressure was ca. 10 Pa and G was equal to 1.07 mW/K. The cell parameters G, $\alpha_0/\sqrt{f}, \alpha_h/\sqrt{f}$, C_0 and C_h were determined in advance without a sample.

Thus, we have five parameters for fitting the experimental dependence $\mathbf{C}_{emp}(T, f)$ by Eq. (6) at any fixed temperature. The experimental dependences of the absolute value $C_{emp}(300\ K, f)$ and the phase shift $\varphi = \arg(1/\mathbf{C}_{emp})$ were in agreement within 3% accuracy with Eq. (6) in the broad frequency range 0.1–100 Hz for the following parameters: $C_0 = 4.3$ mJ/K, $C_h = 2.05$ mJ/K, $\alpha_0/\sqrt{f} = 0.17\ s^{1/2}$, $\alpha_h/\sqrt{f} = 2.19\ s^{1/2}$, $G = 1.07$ mW/K.

Once the cell calibration is performed, the described algorithm makes it possible to carry out simultaneous measurements of the sample's heat capacity and thermal conductivity. The sample's parameters, $\mathbf{C}_s$ and $\boldsymbol{\kappa}_s$, can be determined from the measured, $\mathbf{C}_{01}$ and $\mathbf{C}_{04}$, according to Eqs. (4) and (5).

5. Experimental: complex heat capacity measurements

Further, we focus on the complex heat capacity of polymers in the melting region and consider the approximation of the frequency independent sample's thermal conductivity κ_s. In this approximation the wave vector of the temperature wave in the sample can be expressed as follows: $\mathbf{k}_s = k'_s + i \cdot k''_s$, where $k'_s = k_s \cdot [(1 + \sin\phi)/2]^{1/2}$ and $k'_s = k_s \cdot [(1-\sin\phi)/2]^{1/2}$ as well as $\alpha'_s = \alpha_s \cdot [(1 + \sin\phi)/2]^{1/2}$ and $\alpha''_s = \alpha_s \cdot [(1-\sin\phi)/2]^{1/2}$.

To determine the parameters $\mathrm{Re}(\mathbf{C}_s)$ and $\mathrm{Im}(\mathbf{C}_s)$ simultaneously, it was sufficient to measure the temperature modulation only on one side of the sample. Thus, the subsequent experiments were performed as follows. The temperature-modulation amplitude $\mathbf{T}_A$ was measured on the surface between the sensor and the holder, i.e. $\mathbf{T}_A = \mathbf{T}_{04}$. Therefore, the measured effective heat capacity $\mathbf{C}_{eff} = \mathbf{C}_{04}$ was expressed by Eq. (5). Using this equation, the parameters C_s and ϕ were calculated from the measured C_{eff} and φ.

5.1. Complex heat capacity of polycaprolactone in the melting region

Consider the results for polycaprolactone (PCL). The sample was received from Prof. G.Groenickx (Catholic University of Leuven, Belgium). The molecular weight averages were as follows: the number average $M_n = 34\,000$, the weight average $M_w = 94\,000$ and the polydispersity $M_w/M_n = 2.76$. To avoid any additional phase shift, the sample was placed between the sensor and the heater, without any cuvette. Then, the sample was molten to provide a good thermal contact with substrates. The distance between the substrates was fixed in three points by small glass posts. The sample's thickness was 0.3 mm. This sandwich was pressed with a thin silk thread. The shape of the molten sample was stable due to the surface tension force. The heating and the cooling curves were reproducible after one heating-cooling cycle.

The time lag in the heat transfer through the sample can be estimated as $\tau_s = (C_s d_s)/(S\kappa_s)$, it was ca. 1 s. The apparatus time lag τ_a, in our experiments, was dependent on the output channel of the amplifier. The value τ_a was equal to 5 s at frequencies below 0.5 Hz and 2 s at higher frequencies. Thus, in our experiments, the time lag of the system was determined by the apparatus. The time lag due to the heat transfer through the sample was of no importance.

The temperature dependences of the absolute value C_{eff} and the phase shift $\varphi = \arg(1/\mathbf{C}_{eff})$ for PCL sample of 0.3 mm thickness are shown in Fig. 1. The experiment was performed at the frequency $f = 1$ Hz, the heat-flow rate $P_0 = 9.1$ mW and the amplitude T_A ca. 0.04 K. The sample was cooled from the melt with the underlying rate $q = 5$ K/min and the crystallization at 315 K during 5 min was performed. Then, the melting process was investigated at the heating rate 5 K/min. Of course, there was no melting nor excess heat capacity at cooling, on descending curves in Fig. 1. Thus, it was possible to determine $\kappa_s(T)$ from the descending curves, when $\mathrm{Im}(\mathbf{C}_s) = 0$. The two parameters C_s and κ_s were determined from the measured absolute value C_{eff} and the phase shift φ, using Eq. (5). Analogously, $\kappa_s(T)$ was determined just above the temperature of crystallization, $T_{cr} = 315$ K. The dependence $\kappa_s(T)$ was measured at different frequencies, as shown in the inset of Fig. 1.

These results were in good agreement with the steady-state measurements, which are presented also in the inset of Fig. 1. The steady-state measurements were performed for the same sample in the same cell. The constant heat-flow rate $P_= = 20$ mW was supplied by the heater. The temperature gradient across the sample, $\Delta T_s/d_s$, was measured. The thermal conductivity was obtained from the following relation: $\Delta T_s/d_s = P_=/2S\zeta\kappa_s$, where ζ is the parameter of the

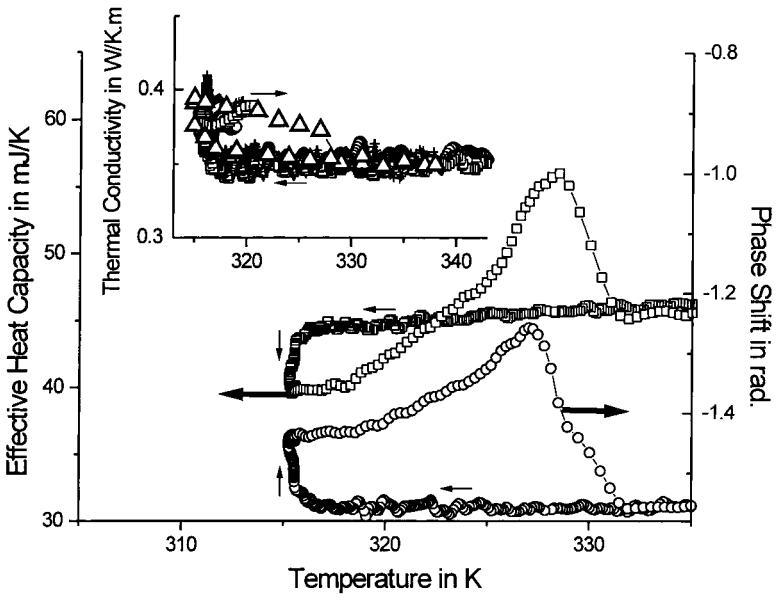

Fig. 1. Temperature dependences of the effective heat capacity C_{eff} and the phase shift $\varphi = \arg(1/\mathbf{C}_{\text{eff}})$ for PCL sample of 0.3 mm thickness. The experiment was performed at the frequency $f = 1$ Hz, the heat-flow rate $P_0 = 9.1$ mW and the amplitude T_A ca. 0.04 K. The sample was cooled from the melt with the underlying rate $q = 5$ K/min and the crystallization at 315 K during 5 min was performed. Then, the melting process was investigated at the heating rate 5 K/min. Temperature dependences of the thermal conductivity κ_s are shown in the inset. The AC measurements were performed at $f = 0.2$ Hz and $T_A = 0.3$ K (squares), 0.4 Hz and 0.12 K (circles), 0.8 Hz and 0.05 K (crosses), and the steady-state measurements of κ_s were performed at heating flow rate $P_= = 20$ mW (triangles).

asymmetry of the cell. In the case of an ideal symmetric cell, when the heat flows symmetrically from the both surfaces of the cell, the parameter ζ equals 1. In our experiments, one surface of the cell was attached to the holder — the silk net. Due to this asymmetry the parameter ζ was equal to 0.75. After normalizing the steady-state data to the parameter ζ, we obtained the results, which were in good agreement with AC measurements beyond the melting region. In the steady-state regime it was possible to measure the static thermal conductivity in the whole temperature range, including the melting region. These measurements show (Fig. 1) that there was no significant change in $\kappa_s(T)$ at melting. Therefore, it was possible to extrapolate the dependence $\kappa_s(T)$, measured beyond the melting region, on the whole temperature range.

Then, the extrapolated dependence $\kappa_s(T)$ was used for the calculations of Re $\mathbf{C}_s(T)$ and Im $\mathbf{C}_s(T)$ from the measured $\mathbf{C}_{\text{eff}}$. The values of κ_s, obtained for amorphous material, were used on the descending part of the curve $\mathbf{C}_{\text{eff}}(T)$ as well as at the end of the melting region of the ascending curve. The values of κ_s, obtained for crystalline material, were used at the beginning of the melting region. Thus, the dependences Re $\mathbf{C}_s(T)$ and Im $\mathbf{C}_s(T)$, shown in Fig. 2, were determined using $\kappa_s(T)$ curves, shown in Fig. 1. Of course, there were discontinuous jumps in the curves of Re $\mathbf{C}_s(T)$ and Im $\mathbf{C}_s(T)$ in the middle of the melting region. As shown in Fig. 2, the discontinuity in Re $\mathbf{C}_s(T)$ was relatively small and this was negligibly small in Im $\mathbf{C}_s(T)$. It appears that the imaginary part, Im $\mathbf{C}_s$, for PCL in the melting region was considerably greater than the real part of the excess heat capacity. This was more apparent at lower frequencies, as shown in Fig. 3 for the same sample.

The linearity of the measurements with respect to modulation amplitude T_A was checked. The measurements were performed at the following amplitudes: $T_A = 0.075$ K and $P_0 = 2.3$ mW, 0.15 K and 4.5 mW, 0.3 K and 9.2 mW. The crystallization at 316 K was for 30 min and the heating–cooling rate was ca. 5 K/min. Nonlinearity was negligible at modulation amplitudes below 0.15 K, but it was noticeable at the amplitude 0.3 K, as shown in Fig. 3.

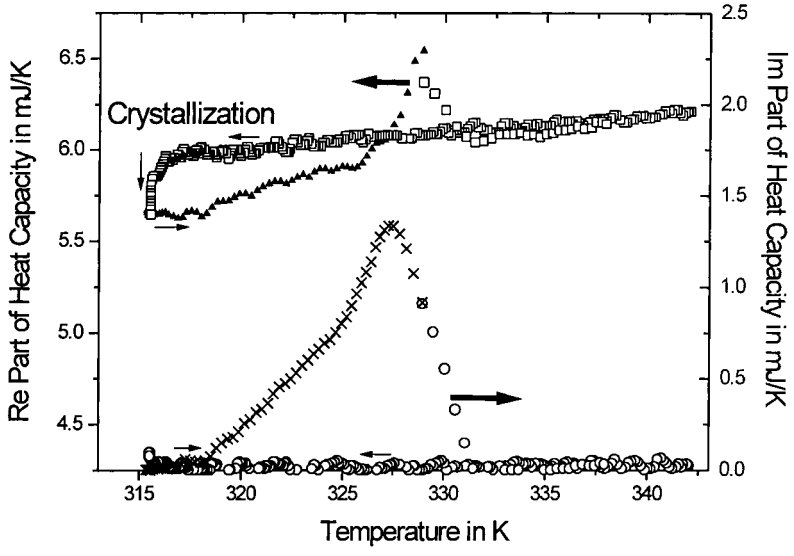

Fig. 2. Temperature dependences of Re $\mathbf{C}_s$ and Im $\mathbf{C}_s$ calculated from the dependences shown in Fig. 1. The values of κ_s, obtained for amorphous material, were used on the descending parts of the curves as well as at the end of the melting region of the ascending curves (open squares and circles). The values of κ_s, obtained for crystalline material, were used at the beginning of the melting region (black triangles and crosses).

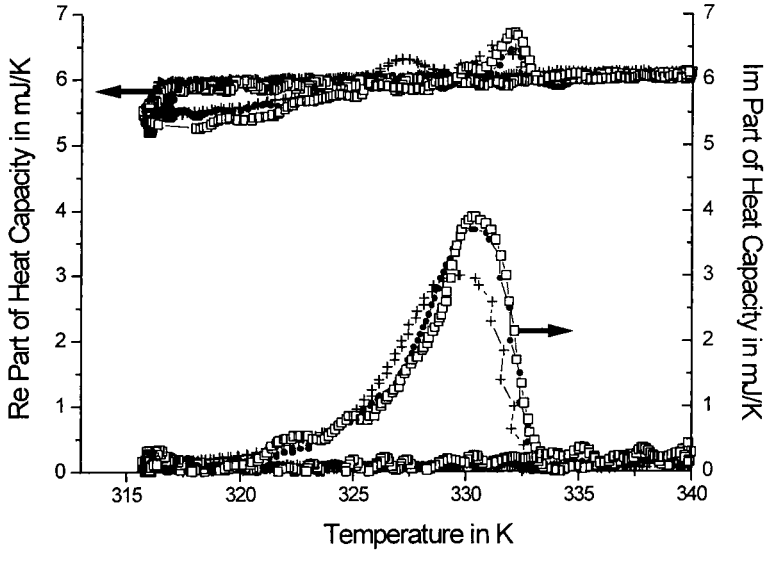

Fig. 3. Temperature dependences of Re $\mathbf{C}_s$ and Im $\mathbf{C}_s$ for the same sample as in Fig. 1. The measurements were performed at $f = 0.2$ Hz and different modulation amplitudes: $T_A = 0.075$ K, $P_0 = 2.3$ mW (squares), 0.15 K, 4.5 mW (circles) and 0.3 K, 9.2 mW (crosses). The sample was cooled from the melt with the underlying rate $q = 5$ K/min and the crystallization at 316 K during 30 min was performed. Then, the melting process was investigated at the heating rate 5 K/min.

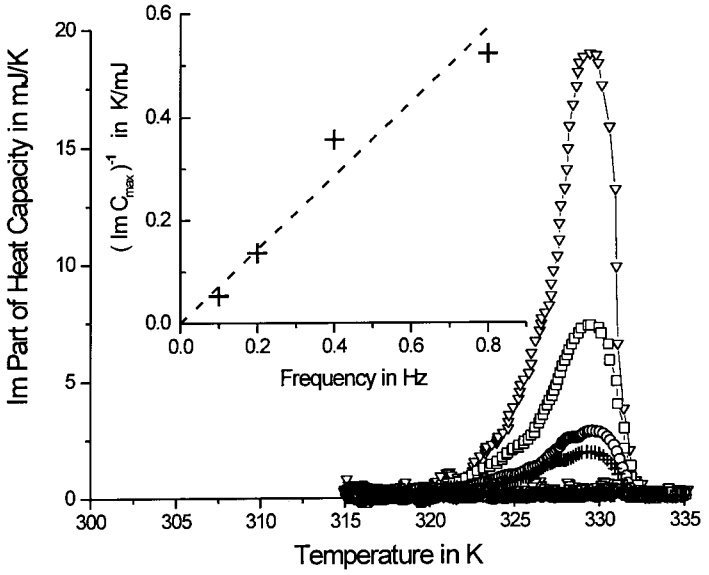

Fig. 4. Temperature dependences of Im $\mathbf{C}_s(\omega)$ for the same sample and the same thermal history as in Fig. 1. The measurements were performed at the following frequencies and amplitudes: $f = 0.1$ Hz and $T_A = 0.1$ K (triangles), 0.2 Hz and 0.1 K (squares), 0.4 Hz and 0.05 K (circles), 0.8 Hz and 0.05 K (crosses). The apparatus time lag, $\tau_a = 5$ s, was the same at all frequencies. Frequency dependence of the inverse maximal value of Im $\mathbf{C}_s(T)$ is shown in the inset.

It was proved in [5,11] that the imaginary part Im $\mathbf{C}_s(\omega) \sim \varepsilon \cdot Q/\omega$ must be measured at melting process, provided irreversible melting exists. Q is the total heat, absorbed by the sample during heating, and $\varepsilon \cdot Q$ is the part of the heat absorbed on heating, which is not released on cooling. A set of the temperature dependences Im $\mathbf{C}_s(T, \omega)$ is shown in Fig. 4 for the following frequencies and modulation amplitudes: $f = 0.1$ Hz and $T_A = 0.1$ K, 0.2 Hz and 0.1 K, 0.4 Hz and 0.05 K, 0.8 Hz and 0.05 K. Denote by Im $\mathbf{C}_{max}$ the maximal value of Im $\mathbf{C}_s(T)$ at the middle of the melting region. The frequency dependence of Im $\mathbf{C}_{max}$ is shown in the inset of Fig. 4. This dependence is in agreement with the relation Im $\mathbf{C}_s \sim 1/\omega$.

Thus, the dynamic excess heat capacity due to completely irreversing melting was observed in PCL. The contribution of the heat-reversing melting was negligibly small.

5.2. Complex heat capacity of 8OCB and water in the melting region

The method was applied to 4.4′-*n*-octyloxycyanobiphenyl (8OCB) liquid crystal in the melting region, smectic–nematic and nematic–isotropic transitions. The sample was received from Merck Ltd. [15]. The arrangement of the sample in the cell was the same as in the previous experiments with PCL. The sample thickness was 0.3 mm.

The measurements were performed at heating–cooling rate ca. 3 K/min. The heating and the cooling curves were reproducible after one heating–cooling cycle. Temperature dependences of the effective heat capacity C_{eff} and the phase shift φ at frequency $f = 1$ Hz are shown in Fig. 5(a). At this frequency the phase shift φ was far from zero. This means that the temperature modulations were not quasi-static. Of course, it was possible to determine the sample's parameters C_s and κ_s using the information on C_{eff} and φ as well as Eq. (5). Note that in the phase transition region, where Im $\mathbf{C}_s \neq 0$, the phase shift φ was the sum of two contributions: ϕ and φ_κ. Thus, the thermal conductivity, determined in this way, contained two physically different contributions. The first was the true thermal conductivity related to φ_κ. The second contribution was related to Im $\mathbf{C}_s$. Therefore, the calculated thermal conductivity should be renamed as the *effective thermal conductivity*, which equals κ_s, when Im $\mathbf{C}_s = 0$. Temperature dependence of the effective thermal conductivity is

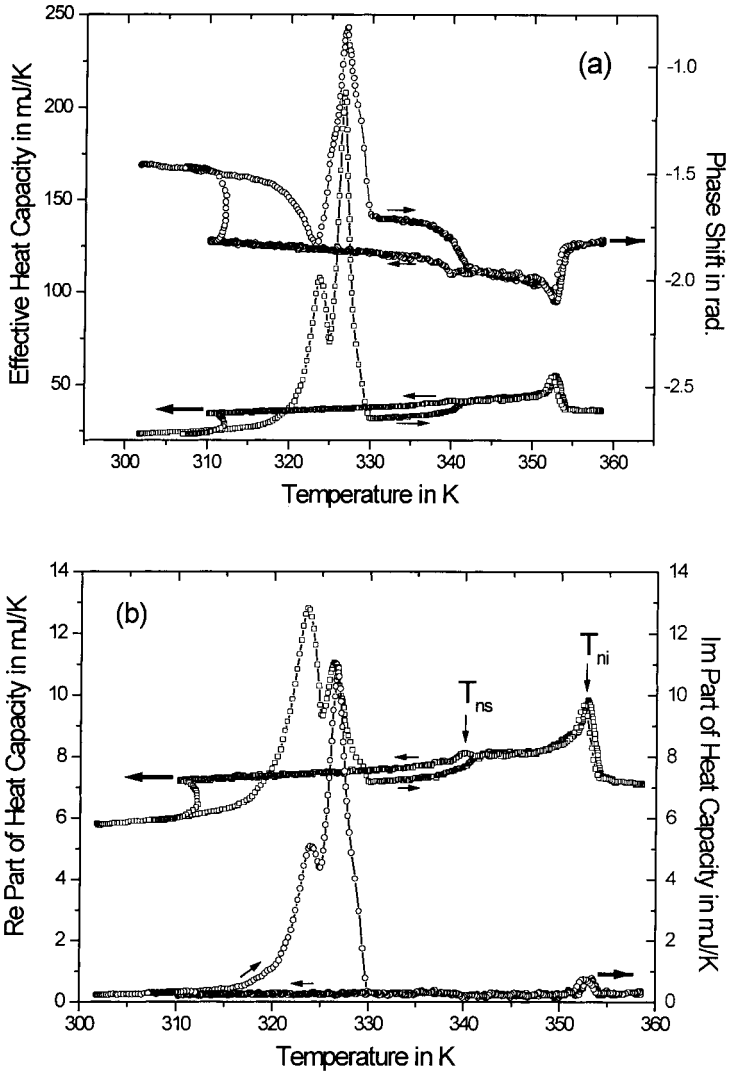

Fig. 5. Temperature dependences of the effective heat capacity C_{eff} and the phase shift φ (a) as well as of Re $\mathbf{C}_s$ and Im $\mathbf{C}_s$ (b) for 8OCB sample of 0.3 mm thickness. The measurements were performed at underlying heating–cooling rate 3 K/min, modulation frequency $f = 1$ Hz, heat-flow amplitude $P_0 = 9.2$ mW and temperature–modulation amplitude T_A ca. 0.035 K.

shown in Fig. 6. This dependence was in agreement with the results of the steady-state measurements in the temperature range beyond phase transitions (Fig. 6). On the other hand, near the phase transitions the large peaks in the effective thermal conductivity were observed. These peaks were related to Im $\mathbf{C}_s$ contribution into the phase shift φ.

The dependences Re $\mathbf{C}_s(T)$ and Im $\mathbf{C}_s(T)$ were determined using the extrapolated $\kappa_s(T)$. A large peak in Im $\mathbf{C}_s(T)$ dependence was observed in the melting region. As shown in Fig. 5(b), the value of Im $\mathbf{C}_s$ was small as compared to Re $\mathbf{C}_s$ at the beginning of the melting process. On the other hand, this value exceeded the real part of the excess heat capacity at the end of the melting region. The fast crystallization with latent heat release and fast spontaneous sample heating was observed at 310 K, as shown in Fig. 5.

The smectic A–nematic and nematic–isotropic transitions at temperatures T_{sn} and T_{ni} were well defined and at the same positions as in [16]. The steps and

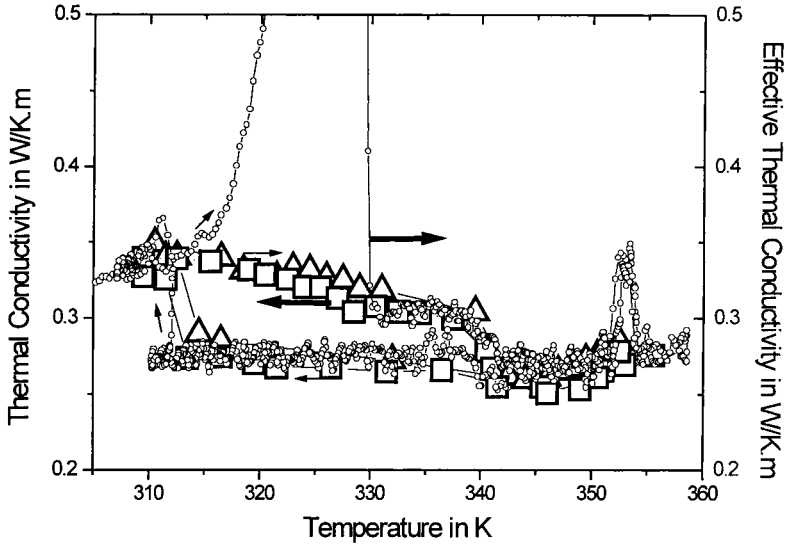

Fig. 6. Temperature dependences of the thermal conductivity for the same sample as in Fig. 5. AC measurements of the effective thermal conductivity (small circles) were performed at the same conditions as in Fig. 5. The steady-state measurements were performed at the heat-flow rate $P_{=} = 20$ mW (squares) and 37 mW (triangles).

peaks in $C_s(T)$ dependence at T_{sn} and T_{ni} were observed. These results were independent of the temperature modulation amplitudes T_A below 0.1 K. The transitions became smeared at P_0 ca. 20 mW and T_A ca. 0.1 K. In this case, the temperature difference $\Delta T_s = 2$ K across the sample was relatively large. The peak of Im $\mathbf{C}_s(T)$ dependence was observed at nematic–isotropic transition, as shown in Fig. 5. It was found that this peak disappeared at relatively high amplitudes $T_A \geq 0.1$ K.

It is noteworthy that the simultaneous measurements of Re $\mathbf{C}_s$ and Im $\mathbf{C}_s$ gave a possibility to distinguish heat-reversing and completely irreversing melting processes. As it was found, the excess heat capacity due to irreversible melting in 8OCB was increased at the end of the melting process. On the contrary, the contribution of the heat-reversing melting was relatively small at the end of the melting region.

Analogous result was obtained at melting of water ice. The sample of distillated water was relatively clean to reveal the super-cooling effect in the temperature interval as large as ca. 14 K. The crystallization was reproducibly observed below 260 K. To avoid any additional phase shift, the measurements were performed without any cuvette. A water drop of volume ca. 10^{-3} cm^3 was placed between the sapphire substrates of the heater and the sensor. The shape of the drop was maintained by the surface tension force. The thickness of the layer of water was ca. 0.1 mm. The thermal conductivity of water was sufficiently large and the temperature modulation was almost quasi-static. Unfortunately, the drop kept evaporating during the experiment and it was impossible to compare the results at different frequencies quantitatively. However, the results were qualitatively reproducible during three or four cycles. The results were qualitatively the same for large, ca. 5×10^{-3} cm^3, and small, ca. 10^{-4} cm^3, drops. Temperature dependences of Re $\mathbf{C}_s$ and Im $\mathbf{C}_s$ are shown in Fig. 7. The measurements were performed at the amplitude $P_0 = 2.3$ mW and modulation frequency $f = 1$ Hz. The underlying heating–cooling rate was ca. 5 K/min at temperatures far from the melting region and ca. 0.3 K/min near the melting transition. The modulation amplitude T_A was ca. 5×10^{-2} K far from the melting region and ca. 10^{-3} K in the melting transition. A long premelting tail was observed at temperatures below $T_c = 273.2$ K. This tail can be attributed to the intergranular defects in the polycrystalline ice [17]. The heat-reversing melting was relatively large in the temperature region from T_c–3 K to T_c and suddenly disappeared after T_c.

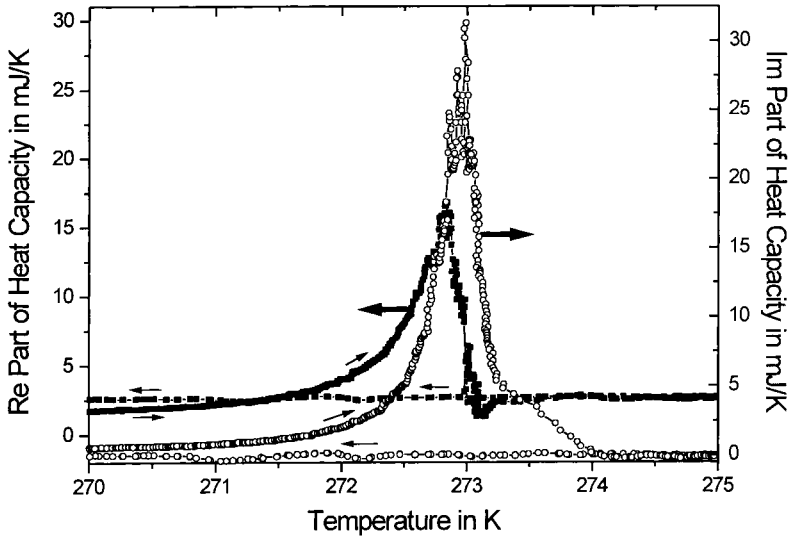

Fig. 7. Temperature dependences of the real and imaginary parts of the complex heat capacity $\mathbf{C}_s$ for water. The measurements were performed for water drop of volume ca. 10^{-3}cm^3 and of thickness ca. 0.1 mm, at frequency 1 Hz, and the amplitude of the heat-flow rate $P_0 = 2.3$ mW. The underlying heating–cooling rate was ca. 5 K/min at temperatures far from the melting region and ca. 0.3 K/min near the melting transition. The modulation amplitude T_A was ca. 5×10^{-2} K far from the melting region and ca. 10^{-3} K in the melting transition.

On the contrary, the completely irreversing melting stayed large on the tail after T_c, where the ice-like short-range order was destroyed irreversibly. Thus, the different physical processes at melting can be distinguished by complex heat capacity measurements.

6. Conclusions

The advanced AC calorimetry, when working at frequencies above the classical limit, can be applied for simultaneous measurements of the complex heat capacity and thermal conductivity. The mathematical algorithm for such measurements was developed. This algorithm can be applied for different materials, when the complex amplitudes of the temperature modulations are measured on both sides of the sample. As a first step, the approximation of the frequency independent thermal conductivity was applied for polymers, when the complex amplitude T_A was measured only on one side of the sample.

It is noteworthy that the simultaneous measurements of Re $\mathbf{C}_s$ and Im $\mathbf{C}_s$ gave a possibility to distinguish reversing [12] (more definitely heat-reversing) and irreversing melting processes. The imaginary part of the complex heat capacity is related to irreversing melting and the real part to heat-reversing melting. As it was shown, the excess heat capacity due to irreversing melting in the liquid crystal 8OCB and in water ice was increased at the end of the melting process. On the contrary, the contribution of the heat-reversing melting was small at the end of the melting region. The contribution of the heat-reversing melting in PCL was relatively small in the whole melting region. The relation Im $\mathbf{C}_s \sim 1/\omega$ was experimentally proved for the melting process in PCL in the frequency range 0.1–1 Hz.

Acknowledgements

This work is financially supported by the European Commission, grant number IC15CT96-0821. The authors gratefully acknowledge Professor G. Salvetti with whom they had fruitful discussions.

References

[1] P.F. Sullivan, G. Seidel, Phys. Rev. 173 (1968) 679.
[2] P. Handler, D.E. Mapother, M. Rayl, Phys. Rev. Lett. 19 (1967) 356.
[3] M.B. Salamon, Phys. Rev. B 2 (1970) 214.

[4] I. Hatta, A. Ikushima, J. Phys. Chem. Solids 34 (1973) 57.
[5] A.A. Minakov, C. Schick, Yu.V. Bugoslavsky, Thermochim. Acta 317 (1998) 117.
[6] A.A. Minakov, C. Sechick, Thermochim Acta, 330 (1999) 109.
[7] J.E.K. Schawe, Thermochim. Acta 304/305 (1997) 111.
[8] Jeong Yoon-Hee, Thermochim. Acta 304/305 (1997) 67.
[9] E. Donth, J. Korus, E. Hempel, M. Beiner, Thermochim. Acta 304/305 (1997) 239.
[10] G.W.H. Hohne, Thermochim. Acta 304/305 (1997) 121.
[11] J.E.K. Schawe, E. Bergmann, Thermochim. Acta 304/305 (1997) 179.
[12] I. Okazaki, B. Wunderlich, Macromoleculare Chemie Rapid Commun. 18 (1997) 313.
[13] A.A. Minakov, Thermochim. Acta 304/305 (1997) 165.
[14] A.A. Minakov, Thermochim. Acta, in print.
[15] Available as M24 from: Merck Ltd., Broom Road, Poole BH12 4NN, UK.
[16] A. Hensel, C. Schick, Thermochim. Acta 304/305 (1997) 229.
[17] G. Salvetti, E. Tombari, G.P. Johari, J. Chem. Phys. 102 (1995) 4987.